Paper presented at the 15th Int. Conf. on General Relativity and Gravitation
Cordoba, Argentina, 1992: Part 1, Plenary Lectures

Applications of numerical relativity: critical behavior and black-hole containing spacetimes

Charles R. Evans

Department of Physics and Astronomy
University of N. Carolina, Chapel Hill, NC 27599

Abstract. Several recent applications of numerical relativity techniques are described. The first is the remarkable evidence of critical phenomena in general relativity associated with gravitational collapse of massless fields. We discuss the two currently known examples of such critical behavior: gravitational collapse of massless scalar field and of axisymmetric gravitational waves. A second application is discussed, in which numerical relativity techniques are used to probe the interaction between strong gravitational waves and black holes. Finally, a numerical approach to computing initial data for spacetimes that contain two black holes is described. Such initial data may ultimately serve as a starting point for the computation of the orbital decay and coalescence of a black hole binary.

1. Introduction

Very near or shortly after the turn of the century, the Laser Interferometer Gravitational-wave Observatory (LIGO) is expected to detect signals from compact binary star systems in their final stages of orbital decay and coalescence [1, 2]. The theoretical foundation for making precise predictions of the phase of the orbit during orbital decay, and using such a prediction to fit observed signals to determine stellar and orbital parameters, is the subject of intense present-day scrutiny [3, 4], as various speakers at the conference have attested. In contrast, theoretical predictions of the signals from the coalescence itself, at least for the coalescence of two black holes, have yet to be made. It seems likely that to make these predictions the full machinery of numerical relativity will be required, and then only after further advances have been achieved in supercomputer technology and additional experience is gained in multidimensional simulations.

Since the development of the cosmic censorship hypothesis [5] over two decades ago, no definitive theorems have been advanced to prove that singularities will always be clothed by event horizons. Nonetheless, support for the conjecture is provided by linear stability analysis of black holes and, with few exceptions, by numerical relativity calculations of gravitational collapse. The latter refers to the fact that in nearly every

gravitational collapse calculation in numerical relativity to date, in which the impending development of a singularity was indicated, an event horizon (and a black hole) has been shown to form. A notable exception is the computation carried out by Shapiro and Teukolsky [6] of collapse of a prolate cluster of collisionless matter. This topic is discussed in some detail by Teukolsky in this volume and will not be addressed further here except to note that cosmic censorship and modeling sources of gravitational radiation are precisely the types of issues that numerical relativity, in principle, can serve to address.

Numerical relativity includes, broadly speaking, any large-scale computational approach to a problem in classical general relativity. It usually refers to calculations of the complete Einstein equations, although a variety of distinct schemes (e.g., spacelike 3+1 [7], 2+2, and null-cone [8] decompositions) have been developed to provide numerical solutions. Occasionally, the term is used to refer to multidimensional Newtonian and post-Newtonian calculations as well, such as Finn's [9] models of gravitational radiation from rotating stellar core collapse and Nakamura and Oohara's and Rasio and Shapiro's [10] simulations of binary neutron star merger. It encompasses applications of Regge calculus also [11]. In general, numerical relativity is used to denote numerical approaches to any problem involving at least two nontrivial dimensions and the solution of partial differential equations. Numerical relativity has as its goal to provide solutions of the field equations in circumstances where an analytic approach is not feasible, which typically means spacetimes that lack a high degree of symmetry or that involve strong, dynamic, and nonlinear fields. Some common applications include *i)* modeling sources of gravitational radiation, *ii)* nonspherical gravitational collapse and explorations of cosmic censorship [6], *iii)* inhomogeneous cosmologies, *iv)* black-hole collisions [12], and *v)* strong gravitational wave–black hole interactions.

While this presentation is meant to be partly in the nature of a review, with so many areas of active research it proved necessary to be somewhat selective in the topics to be treated. I have opted to narrow the focus considerably and review *i)* the very recent discovery of critical phenomena in general relativity, *ii)* numerical models of the interaction between strong gravitational waves and black holes, and *iii)* the numerical construction of initial data for spacetimes containing two black holes (a possible starting point for the coalescence problem). With the focus of the article thus restricted, this discussion unavoidably manages to slight the work of many other researchers and we must instead merely refer the reader to several recent, more-complete, book-length reviews [13, 14].

2. Critical behavior in gravitational collapse

Choptuik [15, 16] recently discovered the existence of critical phenomena in general relativity. The critical behavior is associated with spacetimes that come very close to forming a black hole and those that just manage to do so. Choptuik discovered these effects by computing the gravitational collapse of spherically-symmetric wavepackets of massless scalar field $\phi(r,t)$ using a sensitive finite-difference method. The finite difference code is based upon an adaptive-mesh-refinement algorithm developed by Berger and Oliger [17] that is particularly well suited to follow the development of very fine spatial and temporal features. A second example of critical phenomena has been found by

Abrahams and Evans [18] who considered numerical models of collapse of axisymmetric gravitational waves. These spacetimes were also computed by using a finite difference method, but in this case with a modestly-adjustable moving-mesh algorithm and not with a full adaptive-mesh-refinement scheme.

Some of the characteristics of the critical phenomena seen in these simulations can be summarized in general terms. Critical phenomena become evident in the simulations as variations in the properties of spacetimes across a parameter space of spacetimes. While there are many ways of parameterizing spacetimes, we will restrict attention to parameter spaces that are each described by a single parameter. We can consider a set $\mathcal{G}$ of many such distinct one-dimensional parameter spaces $\mathcal{G}_k$ of spacetimes $\mathcal{S}_k[p_k]$. For each (appropriately defined) parameter space $\mathcal{G}_k$, a critical value $p_k^\star$ of the parameter p_k separates the parameter space into a half space $\mathcal{G}_k^+$ of spacetimes that contain a black hole and a half space $\mathcal{G}_k^-$ of spacetimes that do not. In this way, the parameters p_k are associated with variations in the strength of the ensuing gravitational self-interaction. Critical behavior occurs in a neighborhood of the critical parameter value, when $|p_k - p_k^\star| < \delta_k$, and hence in spacetimes that are just on either side of the "edge" of forming a black hole. Certain features of individual spacetimes display variations across a parameter space that can be considered *critical*. For example, in $\mathcal{G}_k^+$, black-hole mass is found to be a critically-behaving quantity with a power-law dependence $C|p_k - p_k^\star|^\beta$ on the separation of p_k from $p_k^\star$ and with a critical exponent β. The critical behavior of black-hole mass is reminiscent of spontaneous magnetization of ferromagnets in statistical physics, and suggests [18] that black-hole mass plays the rôle of order parameter in general relativity. Near $p_k^\star$, whether a black hole forms or not, the individual spacetimes develop a strong-field region $\mathcal{R}$ that exists during the height of the gravitational self-interaction and within a small enough neighborhood of the center of the implosion. In this strong-field region the gravitational field (and any coupled field) develops an oscillatory character. Close examination of these oscillations has revealed the existence of scaling relations that make successive oscillations echoes of each other on progressively smaller spatial and temporal scales.

Choptuik [16] has been able to demonstrate the *universality* of these critical phenomena in scalar field collapse. (It is likely, but not yet established, that universality is a feature of axisymmetric gravitational wave collapse as well.) To discuss universality the more general space $\mathcal{G}$, of many distinct one-parameter spaces $\mathcal{G}_k$, comes into play. Each $\mathcal{G}_k$ contains a critical spacetime $\mathcal{S}_k[p_k^\star]$ associated with a critical parameter value $p_k^\star$. Universality refers to the fact that, in scalar-field collapse at least, the shape of the fields in the critical solution $\mathcal{S}_k[p_k^\star]$ deep in the strong-field region (and hence the scaling relation) and the value of the critical exponent for black-hole mass both do not depend on which parameter space, $\mathcal{G}_k$, of $\mathcal{G}$ is examined. In other words the critical phenomena are generic features independent of the details of the initial data. The critical exponent and scaling relation may depend, however, on the type of field (e.g., minimally-coupled and non-minimally-coupled scalar fields, electromagnetic field, gravitational field, etc.) that induces the collapse and, in a related fashion, on the degree of symmetry (or nontrivial dimensionality) of the spacetimes, but in ways that are not yet understood. The two known examples of critical phenomena in gravitational collapse illustrate these issues and the present rudimentary state of our knowledge.

2.1. Critical phenomena in massless scalar field collapse

The initial discovery [16] of critical behavior was found by modeling collapse of spherically-symmetric wavepackets of scalar field. The equation of motion of the scalar field is

$$\phi_{;\mu}{}^{;\mu} = \zeta R\phi, \tag{1}$$

and Choptuik considers [15] both minimally-coupled ($\zeta = 0$) and non-minimally-coupled fields. In spherical symmetry, the line element is taken to have the form

$$ds^2 = -\alpha^2(r,t)dt^2 + a^2(r,t)dr^2 + r^2 d\Omega^2, \tag{2}$$

with α the lapse function and a the radial metric function. This gauge is a generalization of Schwarzschild coordinates for dynamical spacetimes. The lapse is fixed by adopting the polar time slicing condition [19] and the spatial coordinate trajectories are fixed to be normal to the time slices by adopting a vanishing shift vector $\beta^r = 0$. Defining auxiliary variables

$$\Phi = \phi', \qquad \Pi = \frac{a}{\alpha}\dot{\phi}, \tag{3}$$

the equations Choptuik solves (in the minimally-coupled case) are

$$\dot{\Phi} = \left(\frac{\alpha}{a}\Pi\right)', \tag{4}$$

$$\dot{\Pi} = \frac{1}{r^2}\left(r^2\frac{\alpha}{a}\Phi\right)', \tag{5}$$

$$\frac{\alpha'}{\alpha} - \frac{a'}{a} + \frac{1-a^2}{r} = 0, \tag{6}$$

$$\frac{a'}{a} + \frac{a^2-1}{2r} - 2\pi r(\Phi^2 + \Pi^2) = 0, \tag{7}$$

where a dot and a prime denote $\partial/\partial t$ and $\partial/\partial r$, respectively. As mentioned before, finite difference equations are obtained from these partial differential equations and solved by using an adaptive-mesh-refinement algorithm. The adaptive-mesh-refinement algorithm dynamically monitors the local truncation errors and maintains a limit on the size of these errors by producing, as needed, local, nested refinements in the mesh in both space and time. Hence, any sharp spatial and temporal features that might develop can be followed with this scheme, whereas they would otherwise become underresolved and lost in a simulation using a fixed mesh.

A typical one-parameter space of solutions is generated from initial (Cauchy) data that takes the scalar field ϕ to have an initial profile

$$\phi(r,0) = \phi_0 r^3 e^{-[(r-r_0)/\Delta]^q}, \tag{8}$$

and demands, as a condition on Π, that the scalar radiation be purely ingoing initially. There are several parameters in these data, but if r_0, Δ and q are considered fixed, then ϕ_0 serves as a single parameter p characterizing the sequence (i.e., a particular subspace

$\mathcal{G}_k$). The initial data are completed by solving the slicing condition (6) for α and the Hamiltonian constraint (7) for a.

The parameter ϕ_0 is monotonically related to the strength of the self-interaction. For small ϕ_0 the wavepacket implodes, passes through itself and then disperses to infinity, while for sufficiently large ϕ_0 the imploding wavepacket forms a black hole. There exists along the sequence a critical value, $\phi_0 = \phi_0^\star$, at which a black hole first appears and which separates supercritical ($\phi_0 > \phi_0^\star$) solutions from subcritical ($\phi_0 < \phi_0^\star$) ones. The solutions of greatest interest are those with parameter values ϕ_0 close to the critical value $\phi_0^\star$. In regions of parameter space near $\phi_0^\star$, Choptuik has found that the natural variable for characterizing variations in parameter space is

$$\pi = \ln|\phi_0 - \phi_0^\star|. \tag{9}$$

Stated another way, critical features in solutions that lie near the critical point tend to depend linearly on π, and therefore *exponentially* on the initial conditions. Additionally, structures with increasingly finer spatial and temporal scales develop as $\phi_0 \to \phi_0^\star$.

The echoing behavior and scaling relation can best be described in terms of two alternative variables, $X = \sqrt{2\pi}r\Phi/a$ and $Y = \sqrt{2\pi}r\Pi/a$, which are useful because they are invariant with respect to rescalings of the length and time coordinates ($r \to \kappa r$ and $t \to \kappa t$), and hence to rescaling of the mass of the spacetime. In near-critical solutions and in the strong-field region, a number of oscillations of the scalar field appear, with their number being proportional to $|\pi|$. It is therefore conjectured that every critical solution (one from each $\mathcal{G}_k$) will contain an infinite number of echoes. To describe why these are echoes and to express the scaling relation, we need logarithmic spatial and temporal coordinates ρ and τ defined by

$$\rho = \ln r, \tag{10}$$

$$\tau = \ln(T^\star - T), \tag{11}$$

where r is the proper (areal) radius and T is the proper time of the central observer at $r = 0$. The constant $T^\star$ is the finite accumulation time of the echoes in the precisely critical solution and is a value that can be determined in near-critical solutions by fitting. Choptuik finds [16] that an approximate scaling relation holds for the oscillations of the scalar field:

$$X(\rho - \Delta, \tau - \Delta) = X(\rho, \tau), \tag{12}$$

$$Y(\rho - \Delta, \tau - \Delta) = Y(\rho, \tau), \tag{13}$$

for a particular logarithmic scaling constant Δ. This makes the oscillations appear as echoes of one another but on scales progressively finer by a factor $e^{-\Delta}$. Stated another way, if we observe the radial profiles of X and Y at some time T_1, which gives a small interval $\delta T_1 = T^\star - T_1$ before $T^\star$ but is otherwise arbitrary, and again at a second time T_2 with the still smaller interval $\delta T_2 = e^{-\Delta}\delta T_1$ before $T^\star$, then a new feature will have appeared in the later profiles on a finer scale but the new profiles are in fact identical to the earlier ones upon rescaling radially by a factor e^{Δ}.

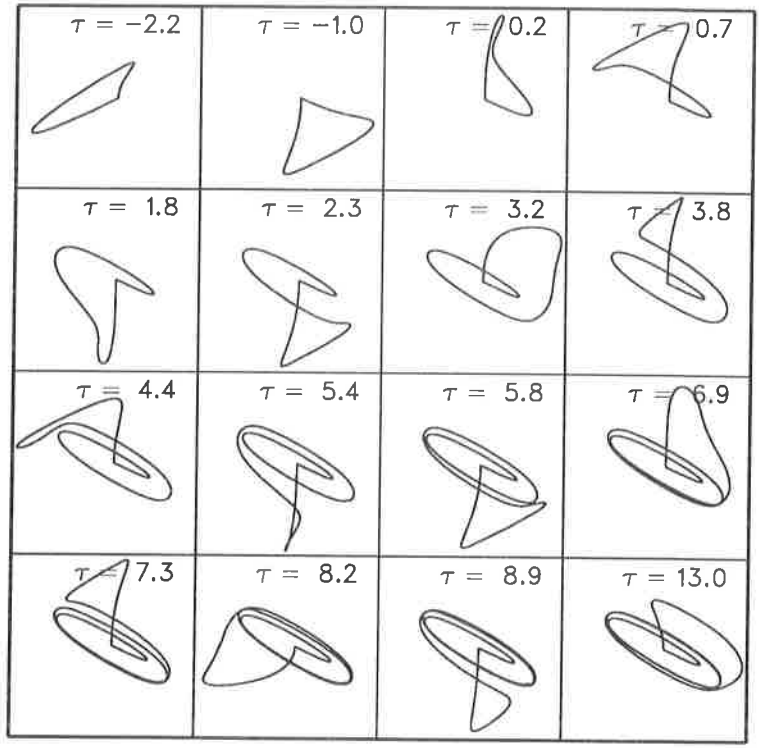

Figure 1. Evolution of the phase portrait of a near-critical solution of the minimally-coupled scalar field–gravity equations. Each portrait is the figure formed by plotting $Y(\rho,\tau)$ versus $X(\rho,\tau)$ at fixed time τ with ρ serving as curve parameter. Phase portraits at successive times are labeled by their values of $|\tau|$. Echoes in the strong-field region appear as self-similar wraps about the nearly elliptical "attractor," whose shape is found to be universal.

The scaling relation is approximate because even in the precisely critical solution the initial oscillations near the outer edge of the strong-field region contain information about the initial data. This information is washed out with each echo, making adherence to the scaling relation progressively tighter. Furthermore, any solution that is near critical, but not precisely critical, will produce only a finite number of echoes as $T^\star$ is approached before it "decides" whether to form a black hole or not.

These echoing properties are illustrated in Figure 1 by plotting, for a particular near-critical solution, the parametric relationship that can be formed between $Y(\rho,\tau)$ and $X(\rho,\tau)$ at fixed time τ with the radial coordinate ρ serving as curve parameter. This produces a phase portrait of the solution at fixed times. The phase portraits at successive times are shown labeled by their values of $|\tau|$. As $T \to T^\star$ a series of oscillations appear, each evident as a loop about $X = Y = 0$. The fact that the loops are self-similar, nearly identically overlapping each other and producing something analogous to an attractor, illustrates the echoing property and the existence of the scaling relation. The value of

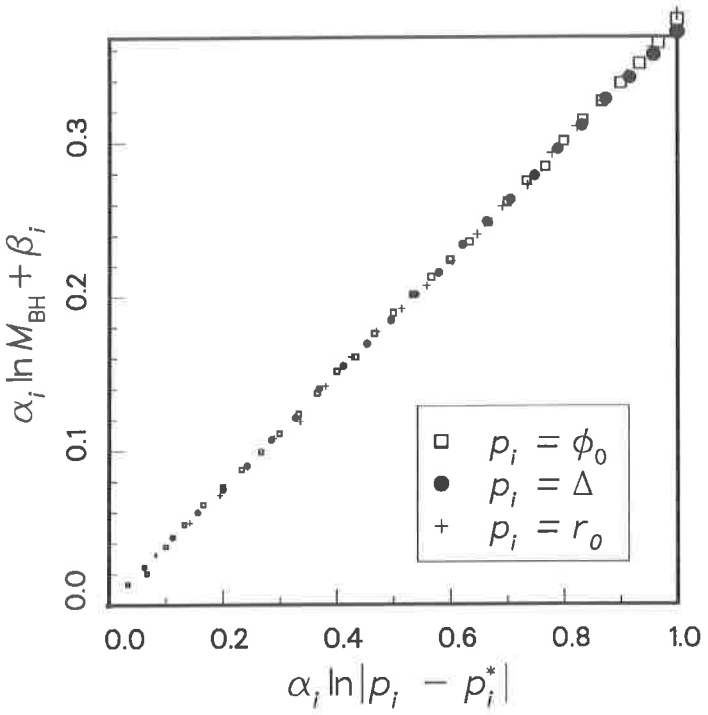

Figure 2. Illustration of the power-law dependence of black-hole mass versus critical separation in parameter space for scalar field collapse. The figure plots $\ln M_{\rm BH}$ versus $\ln(\phi_0 - \phi_0^\star)$. Data from three separate one-parameter spaces are displayed, providing evidence of the universality of the critical behavior of black-hole mass. The slope is the value of the critical exponent, in this case estimated to be $\simeq 0.37$.

Δ in the scaling relation is found to be $\Delta \simeq 3.4$. Both Δ and the profiles, $X(\rho,\tau)$ and $Y(\rho,\tau)$, (and hence the shape of the attractor) are found to be universal, or independent of the family of initial data. Weak dependence on the coupling constant ζ may exist [15].

Equally intriguing behavior is found in one-parameter sequences of solutions from the half-spaces $\mathcal{G}_k^+$ that contain black holes. For the initial data discussed previously, these correspond to $\phi_0 \to \phi_0^\star$ from above. The masses of these black holes have been shown to fit a power law

$$M_{\rm BH} \simeq C|\phi_0 - \phi_0^\star|^\beta, \tag{14}$$

with a critical exponent, $\beta \simeq 0.37$ (see Figure 2). The power-law behavior of $M_{\rm BH}$ is also found to be universal, or independent of the family of initial data, and once again only weak dependence exists, if any, on the coupling constant ζ. The immediate conjecture is that a black hole first appears along any sequence at $p = p^\star$ with infinitesimal mass.

Because of the drastic change in scale with each successive echo ($e^{-\Delta} \simeq 1/30$), the scaling relation probably would not have been discovered without the resolving power afforded by Choptuik's implementation of the Berger-Oliger algorithm. In some of the models Choptuik has computed, the adaptive-mesh-refinement scheme has provided local resolution equivalent to a single uniform grid of 10^9 zones. This has allowed Choptuik to probe points in parameter space with critical separations as small as $|(p-p^*)/p^*| \lesssim 10^{-13}$.

2.2. Critical phenomena in axisymmetric gravitational-wave collapse

Abrahams and Evans [18] have recently found a second example of critical phenomena in general relativity that occurs as axisymmetric *gravitational* wavepackets collapse. These spacetimes are quite distinct physically from Choptuik's spherically-symmetric models of scalar field collapse in two ways: they are source-free, $T^{\mu\nu} = 0$, and have less symmetry (one instead of two Killing vectors). Of course, they also necessarily involve a dynamical degree of freedom of the gravitational field. Several numerical models from a one-parameter family of initial data were discussed at the conference and described elsewhere [20]. While the sequence had a critical parameter value, these particular models each had parameter values far from critical and served merely to show that collapse of gravitational wavepackets would either form a black hole or lead to dispersal of the packet following implosion. In this paper it is now possible to describe the properties of near-critical solutions and to show [18] the existence of critical phenomena similar to that seen in scalar field collapse.

Abrahams and Evans [18] compute axisymmetric, asymptotically-flat vacuum spacetimes using the 3+1 formalism [7]. The coordinates are fixed by adopting the maximal time-slicing condition and the quasi-isotropic spatial gauge. Allowing only one dynamical degree of freedom, the line element takes the form

$$ds^2 = -\alpha^2 dt^2 + \phi^4[e^{2\eta/3}(dr + \beta^r dt)^2$$

$$+r^2 e^{2\eta/3}(d\theta + \beta^\theta dt)^2 + e^{-4\eta/3} r^2 \sin^2\theta d\varphi^2], \tag{15}$$

where α is the lapse function, β^r and β^θ are shift vector components, ϕ is the conformal factor, and η is the even-parity "dynamical" metric function. Maximal slicing results from the condition $K^i{}_i = 0$ on the extrinsic curvature $K^i{}_j$. Abrahams and Evans compute numerical solutions of the following equations:

$$\partial_t \hat{\lambda} = \mathcal{D}_\beta[\hat{\lambda}] - \phi^6(D^r D_r \alpha + 2D^\varphi D_\varphi \alpha)$$

$$+\alpha\phi^6(R^r{}_r + 2R^\varphi{}_\varphi) + \frac{\hat{K}^r{}_\theta}{r}\left[r\partial_r\beta^\theta - \partial_\theta\left(\frac{\beta^r}{r}\right)\right], \tag{16}$$

$$\partial_t \hat{K}^\varphi{}_\varphi = \mathcal{D}_\beta[\hat{K}^\varphi{}_\varphi] - \phi^6 D^\varphi D_\varphi \alpha + \alpha\phi^6 R^\varphi{}_\varphi, \tag{17}$$

$$\partial_t\left(\frac{\hat{K}^r{}_\theta}{r}\right) = \mathcal{D}_\beta\left[\frac{\hat{K}^r{}_\theta}{r}\right] - \frac{1}{r}\phi^6 D^r D_\theta \alpha + \frac{1}{r}\alpha\phi^6 R^r{}_\theta$$

$$+(2\hat{\lambda} - 3\hat{K}^\varphi{}_\varphi)\left[\partial_\theta\left(\frac{\beta^r}{r}\right) - \alpha\frac{K^r{}_\theta}{r}\right], \tag{18}$$

$$\partial_t \eta = \beta^r \partial_r \eta + \beta^\theta \partial_\theta \eta + \partial_\theta \beta^\theta - \beta^\theta \cot\theta + \alpha\lambda, \tag{19}$$

$$\Delta_f^{(3)} \psi = -\frac{1}{4}\psi \left(\Delta_f^{(2)} \eta + \frac{1}{2}\psi^{-8} e^{-2\eta} \hat{K}^i{}_j \hat{K}^j{}_i \right), \tag{20}$$

$$\Delta_f^{(3)} (\alpha\psi) = -\frac{1}{4}\alpha\psi \left(\Delta_f^{(2)} \eta - \frac{7}{2} A^2 K^i{}_j K^j{}_i \right), \tag{21}$$

$$r\partial_r \left(\frac{\beta^r}{r} \right) - \partial_\theta \beta^\theta = \alpha(2\lambda - 3K^\varphi{}_\varphi), \tag{22}$$

$$r\partial_r \beta^\theta + \partial_\theta \left(\frac{\beta^r}{r} \right) = 2\alpha \frac{K^r{}_\theta}{r}, \tag{23}$$

where

$$K^i{}_j K^j{}_i = 2\lambda^2 - 6\lambda K^\varphi{}_\varphi + 6(K^\varphi{}_\varphi)^2 + 2\left(\frac{K^r{}_\theta}{r} \right)^2, \tag{24}$$

and where the transport operator $\mathcal{D}_\beta$ is defined by

$$\mathcal{D}_\beta [u] = \frac{1}{r^2}\partial_r [r^2 \beta^r u] + \frac{1}{\sin\theta}\partial_\theta [\sin\theta \beta^\theta u]. \tag{25}$$

In these equations, $\lambda = K^r{}_r + 2K^\varphi{}_\varphi$, $\hat{K}^i{}_j = \phi^6 K^i{}_j$, D_k is the spatial covariant derivative, $R^i{}_j$ is the spatial Ricci tensor, $A = \phi^2 e^{\eta/3}$, $B = \phi^2 e^{-2\eta/3}$, $\psi = B^{1/2}$ and $\Delta_f^{(3)}$ and $\Delta_f^{(2)}$ are the three- and two-dimensional, flat-space Laplacians, respectively. The analytic properties of this gauge have been discussed previously [21, 22, 19, 23] and the reader is referred to these sources for more details on the coordinates, boundary conditions and asymptotic properties of the gauge. Similarly, portions of the finite difference method have been described elsewhere [21, 22] and will not be elaborated here.

To find Cauchy data for the gravitational field, the freely-specifiable fields, η and $K^r{}_\theta$, are taken to have the form of a *linear* ingoing gravitational wavepacket possessing quadrupolar ($\ell = 2$) angular dependence. The general linear $\ell = 2$ solution is described by a quadrupole moment $I(v)$ of arbitrary profile in advanced time v (or retarded time u). The linear solution involves the quadrupole moment $I(v)$, its first two derivatives, $I^{(1)}(v) \equiv dI(v)/dv$ and $I^{(2)}(v)$, and its integrals, $I^{(-1)}(v) \equiv \int^v dv' I(v')$ and $I^{(-2)}(v)$. Expressions for η and $K^r{}_\theta$ that are consistent with this solution have been found:

$$\eta = \left(\frac{I^{(2)}}{r} - 2\frac{I^{(1)}}{r^2} \right) \sin^2\theta, \tag{26}$$

$$\frac{K^r{}_\theta}{r} = \left(\frac{I^{(2)}}{r^2} - 3\frac{I^{(1)}}{r^3} + 6\frac{I}{r^4} - 6\frac{I^{(-1)}}{r^5} \right) \sin 2\theta. \tag{27}$$

However, since a wavepacket of finite amplitude confined within a finite radius will generate a finite mass, these Cauchy data will be at least slightly nonlinear, depending on the initial amplitude and radius. So to find proper data, the exact Hamiltonian and momentum constraints are solved for ϕ, λ, and $K^\varphi{}_\varphi$, subject to the choice above of η and $K^r{}_\theta$. Not surprisingly, nearly-linear Cauchy data are found still to generate ingoing

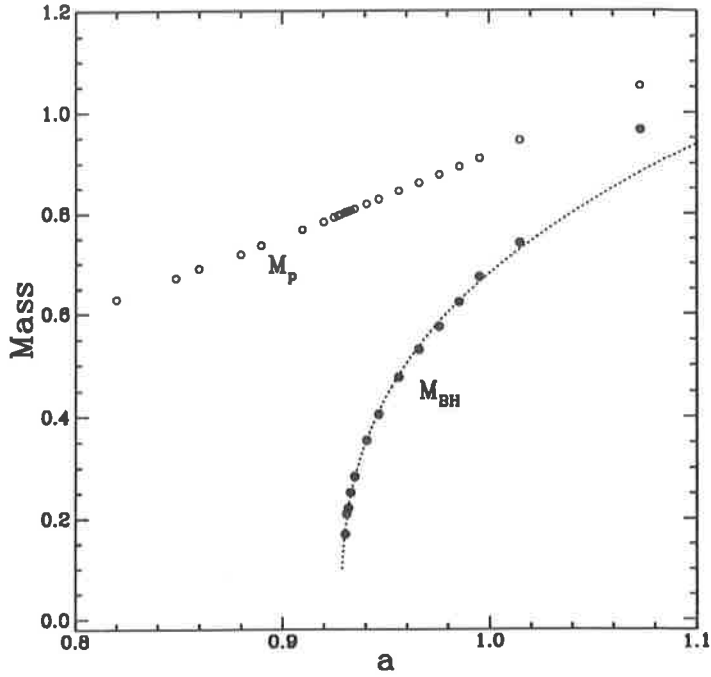

Figure 3. Power-law dependence of black-hole mass versus critical separation in parameter space for axisymmetric gravitational-wave collapse. Remarkably, the value of the critical exponent in this case, $\simeq 0.37$, is indistinguishable from that of scalar field collapse.

solutions. To complete the specification of data, the form of $I(v)$ must be given. A wavepacket with polynomial radial dependence of the form $I^{(-2)}(v) = a\kappa_p L^5[1-(v/L)^2]^6$, for $|v| = |r - r_0| < L$ at $t = 0$, is chosen. Here, κ_p is a constant but a is an amplitude parameter, L is a width parameter, and r_0 is a centering parameter. Each of these might serve as useful parameters of spaces $\mathcal{G}_k$. Initially, L and r_0 have been fixed while a has been chosen to parametrize the Cauchy data and therefore the solutions. Since in the limit $a \to 0$ the mass of the wavepacket is $M_p^{\rm linear} = a^2 L/(2\pi)$, a useful alternative strength parameter is $\Theta(a) = 2\pi M_p/L \simeq a^2$. A wavepacket with $\Theta \ll 1$ only weakly self-interacts [20], escaping to infinity virtually unaffected, while a black hole forms in an evolution where $\Theta \gtrsim 1$, with $M_{\rm BH} \to M_p$ as $\Theta \to \infty$. The critical value along the sequence is found [18] to be $\Theta^\star \simeq 0.80$ ($a^\star \simeq 0.93$).

Like in the scalar field case, supercritical collapse of gravitational wavepackets is found to generate black-hole masses, $M_{\rm BH}$, that are well described by a power law

$$M_{\rm BH} \simeq C(a - a^\star)^\beta. \tag{28}$$

Quite remarkably, the critical exponent value obtained for gravitational wavepacket collapse is also $\beta \simeq 0.37$ and is presently indistinguishable from that seen in scalar field collapse (the estimated numerical uncertainties place the value between 0.35 and 0.39).

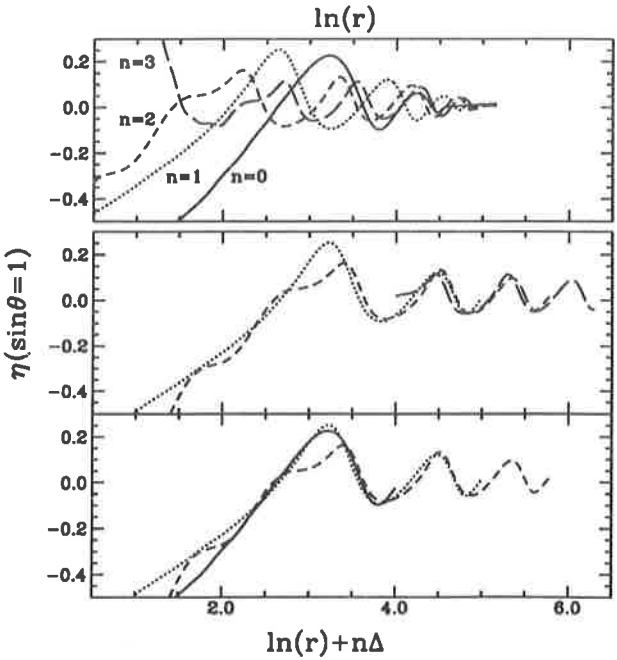

Figure 4. Scaling property of a near-critical solution of axisymmetric gravitational-wave collapse. Radial profiles of the metric function η (along $\theta = \pi/2$) plotted at four times corresponding to alternate maxima of the central value of the lapse function, α_c. The upper panel depicts all four profiles (labeled sequentially $n = 0-3$) plotted versus $\rho = \ln r$. The two lower panels illustrate scaling by overlapping profiles that are shifted by $\rho \to \rho' = \rho + n\Delta$ with $\Delta \simeq 0.6$. Profiles $n = 0, 1, 2$ are plotted in the bottom panel and $n = 1, 2, 3$ in the middle panel.

Figure 3 shows the power-law behavior of black-hole mass found for gravitational-wave collapse. The mass $M_{\rm BH}$ refers to the mass $\sqrt{\mathcal{A}_{ah}/16\pi}$ associated with the area of the apparent horizon $\mathcal{A}_{ah}$, and this is determined at a time $\Delta t = 2\pi/\omega_1^{\ell=2}$ (where $\omega_1^{\ell=2}$ is the real part of the lowest-order $\ell = 2$ quasinormal mode frequency) after the apparent horizon first appears.

Tentative evidence is also observed for a scaling relation on the gravitational field in the strong-field region $\mathcal{R}$. The gravitational field is observed to oscillate on progressively finer spatial and temporal scales. This behavior is evident in examining radial profiles of η (along the equatorial plane $\theta = \pi/2$) as displayed in Figure 4. As can be seen, η exhibits an echoing in $\rho = \ln r$ of the form

$$\eta(\rho - \Delta, t_n) \simeq \eta(\rho, t_{n+1}). \tag{29}$$

The times t_n are found, in this case, by using the central value of the lapse function $\alpha(t, r = 0)$ as a diagnostic to determine the completion of successive oscillations. Once

again a single value of Δ is found to describe the scaling of the echoes. However, in this case, the scaling constant is $\Delta \simeq 0.6$ and it therefore implies a radial scale ratio $e^{\Delta} \simeq 1.8$ which differs considerably from the corresponding value of $e^{\Delta} \simeq 30$ ($\Delta \simeq 3.4$) in scalar-field collapse. This result appears to be robust, having been obtained in simulations with several different resolutions. It is fortunate the scale ratio is much less extreme in this case, since it was obtained using a 2+1 finite difference code without the use of adaptive mesh refinement. Existing 2+1 and proposed 3+1 computations cannot come close to the resolution afforded by adaptive mesh refinement in 1+1, so extension of the adaptive-mesh-refinement scheme to 2D and 3D will be well worthwhile.

2.3. Tentative conclusions

The results obtained so far are suggestive of critical phenomena, but it is fair to ask how close the association really is to standard critical phenomena. Answering this question will likely require the construction of analytic models and more simulations of additional physically-distinct spacetimes with different symmetries and sources. We have seen so far two remarkably similar values of the critical exponent β and two quite different values for the logarithmic scaling factor Δ. The differences may be attributable to the different dimensionalities (or number of Killing vectors) of these two physical models. Do these two physical models then represent different universality classes, despite the nearly identical values of β? The appearance of black holes in only those solutions with $p > p^*$, and the reasonable conjecture that a hole of infinitesimal mass appears at $p = p^*$, suggests that $M_{\rm BH}$ plays the rôle of *order parameter* for these critical phenomena, like spontaneous magnetization M does for ferromagnets below the Curie temperature and like $|\rho - \rho_c|$ does for liquid-gas transitions in the co-existence region. To the extent that $M_{\rm BH}$ can be regarded as the order parameter, it is interesting to note that the critical exponent ($\simeq 0.37$) lies in a range typically observed for β in other critical systems [24]. Choptuik [16] has shown that details inherent in the original data are "washed out" within $\mathcal{R}$ in near-critical evolutions. Information may be steadily lost with each echo as $r \to 0$ and $T \to T^*$ and the rate of loss per echo may depend on the value of Δ. It seems likely that an analogue of the correlation length ξ in statistical systems is the ratio of the radii of the outer edge of the scaling region, $r_{\rm max}$, and the inner edge, r_n, of the innermost echo: i.e., $\xi \sim r_{\rm max}/r_n \sim e^{n\Delta}$. This brings in the scaling variable Δ, and as $p \to p^*$ an ever-larger region (in terms of the scale r_n) becomes "correlated" with self-similar echoes and $\xi \to \infty$.

3. Interaction of black hole spacetimes and gravitational waves

A group of researchers, who are based at or have ties to the US NSF National Center for Supercomputing Applications at the University of Illinois (hereafter called the Illinois group), have recently described [25] numerical models of black-hole spacetimes that interact with finite-amplitude gravitational waves. These are axisymmetric models computed with the Illinois group's new two-dimensional numerical relativity code. This finite difference code also evolves vacuum spacetimes on spacelike time slices by using the 3+1 form of the Einstein equations [7]. The equations for the gravitational field are similar, but not identical to those given in section 2.2.

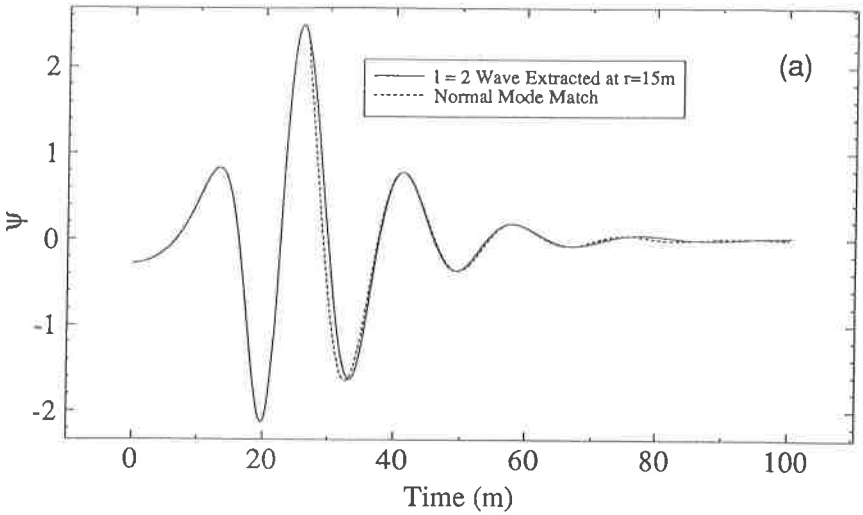

Figure 5. Extracted waveform (solid curve) that is emitted following interaction of a gravitational wave and a black hole. This wave represents a mild but finite amplitude disturbance of the black hole. The normal mode fit (dashed curve) of the waveform is shown to compare well at late times.

The initial data for these models consist of a single black hole superimposed with a time-symmetric gravitational wave (e.g., a Brill wave [26]). The spatial part of the line element takes the form

$$ds^2 = \Psi^4 \left[e^{2q}(d\eta^2 + d\theta^2) + \sin^2\theta \, d\phi^2 \right], \tag{30}$$

where η is a logarithmic radial coordinate. The function $q(\eta, \theta)$ is arbitrary up to satisfying appropriate boundary conditions and $\Psi(\eta, \theta)$ is determined by the Hamiltonian constraint. For $q = 0$ and with an appropriate boundary condition, Ψ becomes the conformal factor for the Schwarzschild solution in isotropic coordinates. When $q \neq 0$ the solution of the Hamiltonian constraint for $\Psi(\eta, \theta)$, along with $q(\eta, \theta)$, corresponds to the superposition of a gravitational wave and a single black hole. Specification of the initial data is completed by assuming time symmetry so that $K_{ij} = 0$. The Brill wave is taken to have the form

$$q = Af(\theta) \left(e^{-[(\eta+\eta_0)/\sigma]^2} + e^{-[(\eta-\eta_0)/\sigma]^2} \right), \tag{31}$$

with parameters A, η_0 and σ specifying the amplitude, range and radial width, respectively. Brill waves with angular dependence $f(\theta) = \sin^n\theta$, for several (even) values of n, have been examined.

The Illinois group describe several simulations with varying initial Brill wave amplitudes and with $n = 4$. Low amplitude Brill waves are shown to excite the fundamental $l = 2$ and $l = 4$ quasi-normal modes of the black hole. The demonstration of an accurate fit by the quasi-normal modes to the late-time behavior of the waveform in these

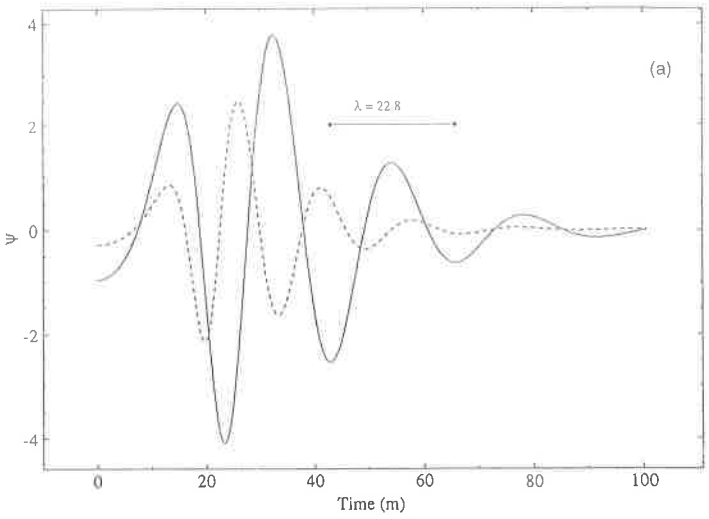

Figure 6. Extracted waveform (solid curve) that is emitted following the interaction between a strong gravitational wave and a black hole. Here the black hole is significantly disturbed by the wave and grows in mass as part of the wave crosses the horizon. The waveform of Figure 5 is overlapped for comparison.

calculations provides an important verification of the code (see Figure 5). A spacetime initially containing a high amplitude Brill wave has also been computed. In this model, the mass associated with the apparent horizon is only 0.59 of the total mass on the initial slice and the initial apparent horizon is observed to be highly distorted. Nevertheless, the gravitational waves shown emerging from the vicinity of the hole quickly develop damped-oscillatory behavior similar to that of quasi-normal modes (Figure 6). The waveform is no longer described well by the quasi-normal modes because the black hole mass grows significantly during the time the waves are being emitted as a significant fraction of the Brill wave is swallowed by the hole. It is as if the initial wave excites oscillations in a bell (the black hole) whose resonance properties are rapidly changing on a time scale of the fundamental oscillation.

In these simulations, the gravitational radiation signal is extracted from data that are available at a finite radius on the spacelike slices. Typically, the fields at distances of $15 - 30M$ from the hole are used to construct a gauge-invariant variable that determines an estimate of the asymptotic waveform. As a check, these researchers also use this boundary data, and data interpolated onto a future-directed null cone, for an integration of the Zerilli equation. The numerically computed Zerilli function, evaluated at larger radii, provides a useful check on the gauge-invariant determination of the waveform.

The intention is to next use this code to compute the head-on collision of two black-holes. This problem was originally studied by Smarr and Eppley [12] over a decade ago, but with less sophisticated techniques and computers. These limitations made it difficult to gauge the accuracy of those calculations. Apart from confirming the previous work,

accurate computation of the axisymmetric collision problem is viewed as a necessary prelude to any attempt to calculate in three dimensions the orbital decay and coalescence of a black-hole binary.

4. Three-dimensional initial data for two black hole collisions

With construction begun on the US Laser Interferometer Gravitational-wave Observatory (LIGO), increasing attention must be devoted to the theoretical task of modeling the orbital decay, coalescence, and gravitational radiation signal of black hole binaries. Before a dynamical evolution can be attempted, initial data must be constructed for the two black holes that satisfies the constraint equations. One means of generating such initial data sets has now been successfully demonstrated [27, 28] that uses the conformal and transverse-traceless decomposition of the constraint equations [7]. This is a conformal imaging procedure that extends Misner's [29] original calculation, of initial data on two asymptotically-flat sheets for a time-symmetric configuration of multiple black holes, to include non-time-symmetric configurations of holes with linear and angular momenta [30, 31, 32].

The procedure involves solving the vacuum Hamiltonian and momentum constraints of 3+1 gravity using the conformal transformations of York [7] to bootstrap into a simultaneous solution. For initial data we take the spatial metric γ_{ij} to be conformally flat, $\gamma_{ij} = \Psi^4\tilde{\gamma}_{ij} = \Psi^4 f_{ij}$ where f_{ij} is the flat three-metric, and the time slice to be maximal $K = K^i{}_i = 0$. The remaining part of the physical extrinsic curvature K_{ij} is then conformally related to the trace-free conformal background extrinsic curvature $\tilde{A}_{ij}$ by $K_{ij} = \Psi^{-2}\tilde{A}_{ij}$. The Hamiltonian and momentum constraints then become

$$\tilde{\nabla}^2\Psi = -\frac{1}{8}\Psi^{-7}\tilde{A}_{ij}\tilde{A}^{ij}, \tag{32}$$

$$\tilde{D}_j\tilde{A}^{ij} = 0, \tag{33}$$

where $\tilde{D}_j$ and $\tilde{\nabla}^2$ are flat-space differential operators. In order for the solutions of these equations to represent black holes, certain boundary conditions have to be assumed. First, boundary conditions are imposed that are consistent with the spacelike slices being asymptotically flat. Second, in order for the source-free equations to describe black holes, the hypersurface must be topologically nontrivial, with each black hole connected to another asymptotically-flat sheet through a throat or Einstein-Rosen bridge. This is the effect of the inner boundary condition used in the work described in the preceding section for one black hole. Here, each black hole on the top sheet may connect to a separate bottom sheet or all of the holes may be connected to the same bottom sheet. The latter approach, with a two-sheeted manifold, has been adopted since it provides an isometry between physical fields on the top and bottom sheets. This isometry implies unique boundary conditions that can be imposed on each of the throats and eliminates the need to include the bottom sheet in the computational domain.

The procedure starts with solutions of the momentum constraint [31] for a single black hole, which have specified (physical) linear and angular momenta:

$$\tilde{A}^p_{ij} = \frac{3}{2r^2}[P_i n_j + P_j n_i - (f_{ij} - n_i n_j)P^k n_k]$$

$$+\frac{3a^2}{2r^4}[P_i n_j + P_j n_i + (f_{ij} - 5n_i n_j)P^k n_k], \tag{34}$$

$$\tilde{A}^s_{ij} = \frac{3}{r^3}(\epsilon_{kim} S^m n^k n_j + \epsilon_{kjm} S^m n^k n_i). \tag{35}$$

The former expression adopts one of two possible isometry conditions (here the negative isometry), which is seemingly most useful physically. The physical linear and angular momenta are given by P^k and S_k, which are not affected by conformal mapping and therefore are not dependent on the solution of the Hamiltonian constraint. These data for $\tilde{A}_{ij}$ are isometric for one hole only. A superposition of two or more such solutions is a solution of the momentum constraint, but does not satisfy the isometry condition. Kulkarni, Shepley and York [32] have shown how higher-order corrections to (34) and (35) can be added, through a method of images for tensors, to construct a solution of the momentum constraint that is inversion symmetric through each hole. This process is rapidly convergent, but analytically nearly intractable. Fortunately, Cook [27] has found a recursive procedure that can be used numerically to generate a discrete solution (i.e., on a computational mesh) to arbitrarily high precision.

Once an inversion-symmetric solution of the momentum constraint is known, the nonlinear Hamiltonian constraint can be solved for Ψ by employing an asymptotically-flat boundary condition $\Psi \to 1$ as $r \to \infty$ and isometry boundary conditions on each of the throats. The conformal factor is then used to "dress" $\tilde{A}_{ij}$ and obtain the physical extrinsic curvature.

Cook [27] has solved these equations for two black hole initial data, subject to the restriction of axisymmetry, for a variety of different black hole linear momenta (aligned along the symmetry axis) and angular momenta (spin axes aligned along the symmetry axis). These results were obtained with two separate finite difference codes, one using Čadež coordinates [33] and one using bispherical coordinates, in order to confirm his results and gauge their precision. In new work, Cook, Choptuik, Dubal, Klasky, Matzner and Oliveira [28] have generalized these results to three dimensions and obtained initial data for two black holes with truly arbitrary linear and angular momenta and masses. Cook and Abrahams [34] have examined these data sets to determine some of the physical properties that are evident on the initial slice, such as asymptotic mass, linear momentum and angular momentum, and areas of apparent horizons.

5. Conclusions

The examples cited here should make evident that numerical relativity has reached a level of sophistication where it is possible both to discover previously unknown physical effects and to state certain results with numerical precision. Even in the interaction of strong gravitational waves with black holes, where we have not yet been surprised with a violation of our physical intuition, the results probe a regime that is far from what we might calculate analytically. Each such solution, where the black hole is strongly perturbed yet fails to produce a naked singularity, lends weight to the notion of relatively generic adherence to the cosmic censorship hypothesis. Finally, the first forays have begun toward designing algorithms and writing codes for three-dimensional numerical relativity calculations. This comes at an opportune time as there are increasing hopes that we will enter the era of gravitational-wave astronomy at the end of the 1990s.

Acknowledgments

The author would like to acknowledge numerous helpful conversations with A. Abrahams, M. Choptuik, G. Cook, E. Seidel and J. York. He is grateful for research support from NSF Grants PHY90-01645 and PHY90-57865 and from the Alfred P. Sloan Foundation.

References

[1] Abramovici, A, Althouse, W E, Drever, R W P, Gürsel, Y, Kawamura, S, Raab, F J, Shoemaker, D, Sievers, L, Spero, R E, Thorne, K S, Vogt, R E, Weiss, R, Whitcomb, S E and Zucker, M E 1992 *Science* **256** 325–33

[2] Abramovici, A 1993, this volume

[3] Cutler, C, Apostolatos, T A, Bildsten, L, Finn, L S, Flanagan, E E, Kennefick, D, Markovic, D M, Ori, A, Poisson, E, Sussman, G J and Thorne, K S 1992 submitted to *Phys. Rev. Lett.*

[4] Cutler, C, Finn, L S, Poisson, E and Sussman, G J 1993 *Phys. Rev.* **D**, in press

[5] Penrose, R, 1969 *Riv. Nuovo Cimento* **1** 252–76

[6] Shapiro, S L and Teukolsky, S A 1991, *Phys. Rev. Lett.* **66** 994–997

[7] York, J W 1979 in *Sources of Gravitational Radiation* (Cambridge: Cambridge University Press) 83–126

[8] Gomez, R, Winicour, J and Isaacson, R A 1992 *J. Comp. Phys.* **98** 11

[9] Finn, L S 1991 in *Nonlinear Problems in Relativity and Cosmology* eds. J Buchler, S Detweiler and J Ipser (New York: New York Acad. Sci.) 156–72

[10] Oohara, K and Nakamura, T 1989 *Prog. Theor. Phys.* **82** 535–54
Nakamura, T and Oohara, K 1989 *Prog. Theor. Phys.* **82** 1066–83
Oohara, K and Nakamura, T 1990 *Prog. Theor. Phys.* **83** 906–40
Nakamura, T and Oohara, K 1991 *Prog. Theor. Phys.* **86** 73–88
Oohara, K and Nakamura, T 1992 *Prog. Theor. Phys.* **88** 307–15
Rasio, F A and Shapiro, S L 1992 *Astrophys. J.* **401** 226–45

[11] Miller, W L 1986, in *Dynamical Spacetimes and Numerical Relativity* edited by J Centrella (Cambridge: Cambridge University Press) 256–303

[12] Smarr, L L 1979, in *Sources of Gravitational Radiation* ed. L L Smarr (Cambridge: Cambridge University Press) 245–74

[13] Evans, C R, Finn, L S and Hobill, D W 1989 *Frontiers in Numerical Relativity* (Cambridge: Cambridge University Press)

[14] d'Inverno, R 1992 *Approaches to Numerical Relativity* (Cambridge: Cambridge University Press)

[15] Choptuik, M W 1992 in *Approaches to Numerical Relativity* edited by R d'Inverno (Cambridge: Cambridge University Press)

[16] Choptuik, M W 1993, *Phys. Rev. Lett.* **70** 9–12

[17] Berger, M J and Oliger, J 1984 *J. Comp. Phys.* **53** 484–512

[18] Abrahams, A M and Evans, C R 1993 submitted to *Phys. Rev. Lett.*

[19] Bardeen, J M and Piran, T 1983 *Phys. Rep.* **96** 205–50

[20] Abrahams, A M and Evans, C R 1992 *Phys. Rev.* **46** R4117–21

[21] Evans, C R 1984 Ph.D. thesis, University of Texas at Austin, unpublished

[22] Evans, C R 1986 in *Dynamical Spacetimes and Numerical Relativity* edited by J Centrella (Cambridge: Cambridge University Press) 3–39

[23] Abrahams, A M and Evans, C R 1988 *Phys. Rev.* **D37** 318–32

[24] Ma, S 1976 *Modern Theory of Critical Phenomena* (Redwood City: Addison-Wesley)

[25] Abrahams, A M, Berstein, D, Hobill, D W, Seidel, E and Smarr, L 1992 *Phys. Rev.* **D45** 3544–58

[26] Brill, D 1959 *Ann. Phys., NY* **7** 466–83

[27] Cook, G B 1991 *Phys. Rev.* **D44** 2983–3000

[28] Cook, G B, Choptuik, M W, Dubal, M R, Klasky, S, Matzner, R A and Oliveira, S R 1993 *Phys. Rev.* **D**, in press

[29] Misner, C W 1963 *Ann. Phys., NY* **24** 102–17

[30] Bowen, J 1979 *Gen. Rel. Grav.* **11** 227–31

[31] Bowen, J and York, J W 1980 *Phys. Rev.* **D21** 2047–56

[32] Kulkarni, A, Shepley, L and York, J W 1983 *Phys. Lett.* **96A** 228–30

[33] Čadež, A 1971 Ph.D. thesis, University of North Carolina, unpublished

[34] Cook, G B and Abrahams, A M 1992 *Phys. Rev.* **D46** 702–13